J. Fluid Mech. (2013), *vol.* 715, *pp.* 32–59.
doi:10.1017/jfm.2012.492

Interphasial energy transfer and particle dissipation in particle-laden wall turbulence

Lihao Zhao[1],†, **Helge I. Andersson**[1] **and Jurriaan J. J. Gillissen**[2]

[1]Department of Energy and Process Engineering, Norwegian University of Science and Technology, 7491 Trondheim, Norway

[2]Department of Chemical Engineering, Delft University of Technology, Leeghwaterstraat 39, 2628 CB Delft, The Netherlands

(Received 19 December 2011; revised 13 August 2012; accepted 4 October 2012)

Transfer of mechanical energy between solid spherical particles and a Newtonian carrier fluid has been explored in two-way coupled direct numerical simulations of turbulent channel flow. The inertial particles have been treated as individual point particles in a Lagrangian framework and their feedback on the fluid phase has been incorporated in the Navier–Stokes equations. At sufficiently large particle response times the Reynolds shear stress and the turbulence intensities in the spanwise and wall-normal directions were attenuated whereas the velocity fluctuations were augmented in the streamwise direction. The physical mechanisms involved in the particle–fluid interactions were analysed in detail, and it was observed that the fluid transferred energy to the particles in the core region of the channel whereas the fluid received kinetic energy from the particles in the wall region. A local imbalance in the work performed by the particles on the fluid and the work exerted by the fluid on the particles was observed. This imbalance gave rise to a particle-induced energy dissipation which represents a loss of mechanical energy from the fluid–particle suspension. An independent examination of the work associated with the different directional components of the Stokes force revealed that the dominating energy transfer was associated with the streamwise component. Both the mean and fluctuating parts of the Stokes force promoted streamwise fluctuations in the near-wall region. The kinetic energy associated with the cross-sectional velocity components was damped due to work done by the particles, and the energy was dissipated rather than recovered as particle kinetic energy. Componentwise scatter plots of the instantaneous velocity versus the instantaneous slip-velocity provided further insight into the energy transfer mechanisms, and the observed modulations of the flow field could thereby be explained.

Key words: multiphase and particle-laden flows, turbulence simulation

1. Introduction

Particle-laden flows frequently occur in the local environment as well as in numerous industrial applications. Turbulent flow of particle suspensions has been extensively studied during the past few decades with a variety of different motivations.

† Email address for correspondence: lihao.zhao@ntnu.no

Either attenuation or augmentation of the turbulent kinetic energy in the presence of solid particles has been observed both in laboratory experiments and numerical computer simulations. Rashidi, Hetsroni & Banerjee (1990) performed measurements with two different sizes of polystyrene particles in wall turbulence, and observed that the larger particles increased the number of wall ejections and also enhanced the Reynolds shear stress. The smallest particles, on the other hand, turned out to have the opposite effect on the turbulence. Kulick, Fessler & Eaton (1994) conducted experiments in a vertical downward channel flow with small heavy particles. Their data indicated that the degree of turbulence attenuation increased with the Stokes number and the mass loading of the particles. From their experimental study Hussainov *et al.* (2000) also reported an attenuation of the turbulence intensity as well as a reduction of the energy density at high frequencies in the presence of small glass beads. In two-way coupled numerical simulations Squires & Eaton (1990), Elghobashi & Truesdell (1993) and Truesdell & Elghobashi (1994) focused on the turbulence modulation in homogeneous isotropic turbulence. Squires & Eaton (1990) observed an increased dissipation rate in the presence of small particles, and the attenuation of the turbulent kinetic energy increased with higher mass loadings. Numerical studies have also explored particle dynamics and transport in wall-bounded turbulence. Pan & Banerjee (1996) carried out two-way coupled simulations by means of direct numerical simulation (DNS), and observed a suppression of the sweeps due to the smaller particles but an enhanced sweep activity in the presence of larger particles. Yamamoto *et al.* (2001) performed a large-eddy simulation (LES) of turbulent gas-particle flow in a vertical channel with four-way coupling, and obtained good agreement with the experimentally observed attenuation of the turbulence for small Stokes numbers. Li *et al.* (2001) performed two-way coupled DNSs and found an increased flow rate in the presence of small particles as well as enhanced velocity fluctuations in the streamwise direction, whereas the turbulence intensities in the two other directions were damped. Both two-way and four-way coupled simulations of particle-laden pipe flow were conducted by Vreman (2007). Various different aspects of particle-laden wall-bounded turbulence have been considered. Dritselis & Vlachos (2008, 2011), for instance, focused on the coherent structures around the wall region and found that the diameter and the streamwise extent of the mean vortices were increased due to the momentum exchange between the particles and fluid. More recently Bijlard *et al.* (2010) studied the topology of the local flow around solid particles and observed that the turbulent flow became more two-dimensional in the viscous sublayer in two-way coupled simulations. This phenomenon was ascribed to the feedback from the particles on the local fluid.

According to earlier findings, small inertial particles tend to attenuate the turbulent kinetic energy whereas larger particles enhance the turbulent energy of the fluid. Even in dilute particle suspensions, several different factors may contribute to the attenuation or augmentation of the fluid turbulence. These physical mechanisms include the kinetic energy transfer between the particles and fluid, the extra dissipation induced by the particles, and the wake formation and eventual vortex shedding behind the particles. Gore & Crowe (1989) proposed a dimensionless parameter, i.e. the ratio of the particle diameter to a characteristic size of the large eddies, to distinguish between augmentation and attenuation of the turbulence. More recently Tanaka & Eaton (2008) proposed a new dimensionless parameter, the so-called particle moment number, in order to categorize the turbulence modulations. Furthermore, as discussed also by Balachandar & Eaton (2010), turbulence attenuation may occur: (i) when the particle inertia increases; or (ii) when there is increased energy dissipation in the immediate

vicinity of the particles; or (iii) if the effective viscosity of the suspension is enhanced. On the contrary, the formation of a wake and vortex shedding behind the particles can lead to an increased turbulence level, and this happens typically when the particle Reynolds number exceeds one hundred.

In spite of the many earlier studies on particle-laden turbulent flows, the underlying physical mechanisms of the turbulence attenuation in the presence of small solid particles are still not fully understood. One may wonder, for instance, if this damping of the turbulent kinetic energy is caused by a reduced energy production or an increased energy dissipation. The point particle two-way coupled approach implemented both in DNS and LES codes enables a close look at the complex interactions between the point particles and the surrounding fluid. Such two-way coupled simulations of turbulent channel and pipe flows have been carried out, for instance, by Pan & Banerjee (1996), Li *et al.* (2001), Rani, Winkler & Vanka (2004) and Zhao, Andersson & Gillissen (2010), but with rather different aims and focus of attention.

In the present computational study of particle-laden channel flow, the focus is on the interactions between the fluid turbulence and the inertial point particles. Two-way coupled point particle Eulerian–Lagrangian direct numerical simulations will be performed. The size of the particles is smaller than the smallest eddies in the turbulence. Five different simulations are performed with a view to studying the influence of the particle characteristics, i.e. particle volume fraction and particle response time, on the particle–turbulence interactions. Data from one of the simulations are further analysed in order to explore the kinetic energy exchange between the particles and local fluid as well as the extra energy dissipation caused by the particles. The mechanical energy exchanged between the two phases are examined by means of instantaneous data in a cross-sectional plane, long-time averages of the transferred power, as well as scatter plots of the flow variables involved. This approach enables us to pinpoint the different roles of the streamwise and cross-sectional components of the fluctuating slip velocity vector.

2. Mathematical model and methodology

2.1. *Eulerian fluid representation*

Turbulent channel flow is studied by means of DNS, which implies that the Navier–Stokes equation in an Eulerian frame of reference is integrated in time and three-dimensional space on a grid sufficiently fine to resolve all scales of the turbulent motion. The motion of the incompressible and isothermal fluid is governed by the mass and momentum conservation equations

$$\boldsymbol{\nabla}\cdot\boldsymbol{u}=0,\quad \rho\left[\frac{\partial \boldsymbol{u}}{\partial t}+(\boldsymbol{u}\cdot\boldsymbol{\nabla})\,\boldsymbol{u}\right]=-\boldsymbol{\nabla}p+\mu\nabla^2\boldsymbol{u}+\boldsymbol{f}^P, \tag{2.1}$$

where $\boldsymbol{u}$ and p are the instantaneous fluid velocity vector and pressure, respectively. The flow is driven in the streamwise direction by a constant negative mean pressure gradient $\boldsymbol{\nabla}P$. In two-way coupled simulations, the last term $\boldsymbol{f}^P$ is added in the momentum equation and represents the feedback force per unit volume due to the presence of the particles. Moreover, ρ and μ are the density and dynamic viscosity of the Newtonian carrier fluid.

To facilitate the subsequent data analysis and also the presentation of the results, the Reynolds decomposition is introduced. The instantaneous fluid velocity components

are decomposed in mean ($\boldsymbol{U}$) and fluctuating ($\tilde{\boldsymbol{u}}$) parts. Correlations between two fluctuating quantities are denoted by an overbar.

2.2. *Reynolds stress budgets in particle-laden flow*

If the Navier–Stokes equation for particle-laden fluid flow (2.1) is written in Cartesian tensor notation, the following transport equation for the second moments $\overline{\tilde{u}_i\tilde{u}_j}$ of the velocity fluctuations can be derived:

$$\frac{\mathrm{D}\overline{\tilde{u}_i\tilde{u}_j}}{\mathrm{D}t} = P_{ij} + B_{ij} + D_{ij} + \Phi_{ij} - \varepsilon_{ij}. \tag{2.2}$$

Here, $\tilde{u}_i$ denotes the component of the fluctuating part of the velocity vector in the x_i-direction and U_i is the corresponding mean velocity. The tensorial terms on the right-hand side represent different physical mechanisms tending to change $\overline{\tilde{u}_i\tilde{u}_j}$, namely production due to mean shear $\boldsymbol{P}$, production due to particle–fluid interaction forces $\boldsymbol{B}$, turbulent and viscous diffusion $\boldsymbol{D}$, pressure–strain interactions $\boldsymbol{\Phi}$, and viscous energy dissipation $\boldsymbol{\varepsilon}$, respectively. In the present study the focus is on the two production terms:

$$P_{ij} = -\overline{\tilde{u}_i\tilde{u}_k}\frac{\partial U_j}{\partial x_k} - \overline{\tilde{u}_j\tilde{u}_k}\frac{\partial U_i}{\partial x_k}, \tag{2.3}$$

$$B_{ij} = \overline{\tilde{u}_i\tilde{f}_j^P} + \overline{\tilde{u}_j\tilde{f}_i^P}. \tag{2.4}$$

The former is present in all turbulent shear flows and represents the production of turbulence caused by interactions between the Reynolds stress components and the mean flow gradients. The second term represents interactions between the fluctuating part of the velocity field and the fluctuating part of the particle–fluid interaction force $\tilde{\boldsymbol{f}}^P$.

The second-moment equation (2.2) in the presence of body forces can be found, for instance, in Hanjalic & Launder (2011). They distinguished between three distinctly different body forces, namely a buoyancy force, a magnetic force, and a Coriolis force. In the present context, however, the body force $\boldsymbol{f}^P$ is the reaction force from the particles onto the fluid.

2.3. *Lagrangian particle dynamics*

The particles in the flow are represented by means of the Lagrangian point particle approach; see e.g. Balachandar & Eaton (2010). Each individual particle is tracked at every time step of the DNS, i.e. the particle velocity and the particle position are altered in accordance with Newtonian dynamics and kinematics. The translational motion of the individual spherical particles is only affected by the Stokes drag force in the present work, while other forces, such as gravity, lift and virtual-mass forces, are neglected. The size of the particles is smaller than the smallest eddy scales in the flow field and, consequently, the force on a particle can be simply treated as a point force. The Stokes drag force on a given spherical particle with radius a is expressed as

$$\boldsymbol{F} = 6\pi\mu a\left[\boldsymbol{u}\left(\boldsymbol{x}_p, t\right) - \boldsymbol{v}\right], \tag{2.5}$$

where $\boldsymbol{u}$ is the local fluid velocity evaluated at the particle location $\boldsymbol{x}_p$ at time t and $\boldsymbol{v}$ is the velocity of the particle. The local fluid velocity is obtained by interpolation using discrete velocity data from the surrounding 27 grid points onto the particle position $\boldsymbol{x}_p$. The position of a particle and its translational velocity can be obtained

from

$$\frac{\mathrm{d}\boldsymbol{x}}{\mathrm{d}t} = \boldsymbol{v}, \quad \frac{\mathrm{d}\boldsymbol{v}}{\mathrm{d}t} = \frac{1}{\tau}\left[\boldsymbol{u}\left(\boldsymbol{x}_p, t\right) - \boldsymbol{v}\right], \quad \tau = \frac{2\rho D a^2}{9\mu}, \tag{2.6}$$

where τ is the particle response time and $D = \rho_p/\rho$ is the density ratio between the particles and the fluid.

The Lagrangian particle equations (2.6) are integrated forward in time with the same time step as the Eulerian fluid equation (2.1) in the course of the simulation. According to Newton's third law, each and every particle acts back onto the local fluid with a point force $-\boldsymbol{F}_l$. The subscript l refers to the particle number. The feedback force on the fluid from n_p particles within a given cell volume V_{cell} can be summed to give

$$\boldsymbol{f}^P = -\frac{1}{V_{cell}} \sum_{l=1}^{n_p} \boldsymbol{F}_l. \tag{2.7}$$

This is the expression of the force per unit volume which appears in the fluid momentum equation (2.1). This two-way coupled scheme in the point particle approach is essentially the same as that followed by Squires & Eaton (1990) in the simulation of isotropic turbulence, and later by Li *et al.* (2001), Picciotto *et al.* (2006), Dritselis & Vlachos (2008) and Zhao *et al.* (2010) for particle-laden turbulent channel flows.

In the present investigation we aim to investigate the subtle effects of inertial point particles on wall turbulence. The gravity force has therefore not been taken into consideration. By ignoring all other forces than the Stokes drag a particularly simple system is left, which is amenable to an in-depth analysis of particle–turbulence interactions. For the same reason, particle–particle interactions are not taken into account.

3. Kinetic energy transfer, conversion and dissipation

The transfer of kinetic energy between the particle phase and the fluid phase in particle-laden flows is of primary concern in the present work. A mathematical analysis of the relationship between the work done by the particles on the surrounding fluid and the work by the local fluid on the particles is provided in this section. The outcome of the analysis will be used in interpretation of the results from the direct numerical simulations in § 6.

The mechanical work done by a force on an object is given by the dot product of the force vector and the displacement vector. In our two-way coupled simulations, the only linkage between the fluid and the particles is the Stokes drag force as given in (2.5) and the reaction force in (2.7). Based on Newton's third law, the point force on a particle $\boldsymbol{F}$ and the force on the local fluid $-\boldsymbol{F}$ always have exactly the same magnitude but opposite directions. The work W^P done by the local fluid to move a particle a distance $\boldsymbol{L}^P = \boldsymbol{v}\,\mathrm{d}t$ during one time step $\mathrm{d}t$ can be expressed as

$$W^P = \boldsymbol{F}\cdot\boldsymbol{L}^P = \boldsymbol{F}\cdot\boldsymbol{v}\,\mathrm{d}t = 6\pi\mu a\left[\boldsymbol{u}(\boldsymbol{x}_p, t) - \boldsymbol{v}\right]\cdot\boldsymbol{v}\,\mathrm{d}t. \tag{3.1}$$

The time rate of the work, i.e. the power, is denoted by a dot and is thus defined by $\dot{W}^P = W^P/\mathrm{d}t$. In order to distinguish between the power associated with motions in different directions, the subscript β is introduced to identify a particular coordinate

direction. The power associated with the motion in the β-direction can be written as

$$\dot{W}^P_\beta = 6\pi\mu a[u_\beta - v_\beta]v_\beta = \alpha\left[u_\beta - v_\beta\right]v_\beta. \tag{3.2}$$

The usual summation convention does not apply to repeated Greek indices. The constant coefficient $\alpha = m_P/\tau = 6\pi\mu a$ is introduced to simplify the expressions; α is defined as the ratio between the particle mass and the particle response time and is thus expressed in kg s^{-1}. In a given case $\dot{W}^P$ is only dependent on the particle velocity and the slip velocity between particle and local fluid. The following quadrant analysis distinguishes between negative and positive power:

$$\begin{aligned}
&(1)\begin{cases}(u_\beta - v_\beta) > 0\\ v_\beta > 0\end{cases} \implies \dot{W}^P_\beta > 0,\\
&(2)\begin{cases}(u_\beta - v_\beta) > 0\\ v_\beta < 0\end{cases} \implies \dot{W}^P_\beta < 0,\\
&(3)\begin{cases}(u_\beta - v_\beta) < 0\\ v_\beta < 0\end{cases} \implies \dot{W}^P_\beta > 0,\\
&(4)\begin{cases}(u_\beta - v_\beta) < 0\\ v_\beta > 0\end{cases} \implies \dot{W}^P_\beta < 0.
\end{aligned} \tag{3.3}$$

A positive power $\dot{W}^P$ means that the local fluid exerts work on the particle, whereas $\dot{W}^P < 0$ implies that the work performed by the fluid on the particles is negative. This scheme will be used to explore the exchange of mechanical energy between the particle phase and the fluid phase in § 6.

Similarly, the work W^f done by a particle to move the local fluid a distance $\boldsymbol{L}^f = \boldsymbol{u}\,\mathrm{d}t$ during one time step is

$$W^f = -\boldsymbol{F}(\boldsymbol{x}_p)\cdot\boldsymbol{L}^f = -\boldsymbol{F}_i(\boldsymbol{x}_p)\cdot\boldsymbol{u}(\boldsymbol{x}_p,t)\,\mathrm{d}t = -6\pi\mu a\left[\boldsymbol{u}(\boldsymbol{x}_p,t) - \boldsymbol{v}\right]\cdot\boldsymbol{u}(\boldsymbol{x}_p,t)\,\mathrm{d}t. \tag{3.4}$$

The associated power $\dot{W}^f = W^f/\mathrm{d}t$ becomes

$$\dot{W}^f_\beta = -6\pi\mu a\left[u_\beta - v_\beta\right]u_\beta = -\alpha\left[u_\beta - v_\beta\right]u_\beta. \tag{3.5}$$

Once again, positive and negative power supply can be analysed similarly as in (3.3).

The sum of $\dot{W}^f$ and $\dot{W}^P$ represents the net loss or gain of mechanical energy per unit time. By summing up over all three coordinate directions, we obtain

$$\dot{W}^f + \dot{W}^P = -\alpha(\boldsymbol{u} - \boldsymbol{v})\cdot(\boldsymbol{u} - \boldsymbol{v}) \equiv -\varepsilon^P \leqslant 0. \tag{3.6}$$

This sum is always negative, which implies that mechanical energy is continuously drained from the fluid–particle suspension due to fluid–particle interactions. The drainage of mechanical energy, or more specifically the loss of kinetic energy, can be interpreted as *particle dissipation* ε^P. The particle dissipation is unconditionally positive, irrespective of whether mechanical energy is transferred from the particles to the fluid or vice versa. This extra dissipation plays an important role in turbulence modulations and can possibly lead to a reduction of the turbulent kinetic energy of the carrier fluid in the spanwise and wall-normal directions and an attenuation of particle fluctuations in the streamwise direction, as will be shown later in this paper.

It is convenient to introduce the Reynolds decomposition for the particle velocity too, by analogy with the fluid velocity in § 2. The instantaneous particle velocity

components are thus decomposed into mean ($\boldsymbol{V}$) and fluctuating ($\tilde{\boldsymbol{v}}$) parts. Let us now introduce this decomposition in (3.2) for the power transferred from the fluid to the particles. After averaging (denoted by an overbar), we obtain

$$\begin{aligned}\overline{\dot{W}_\beta^P} &= \alpha \overline{\left[(U_\beta + \tilde{u}_\beta) - (V_\beta + \tilde{v}_\beta)\right](V_\beta + \tilde{v}_\beta)} \\ &= \alpha \left[\underbrace{(U_\beta - V_\beta)V_\beta}_{\mathrm{I}} + \underbrace{\overline{(U_\beta - V_\beta)\tilde{v}_\beta} + \overline{(\tilde{u}_\beta - \tilde{v}_\beta)V_\beta}}_{=0} + \underbrace{\overline{(\tilde{u}_\beta - \tilde{v}_\beta)\tilde{v}_\beta}}_{\mathrm{II}} \right]. \end{aligned} \tag{3.7}$$

Here, the first term (I) results from work performed by the mean Stokes force on the particles whereas the last term (II) stems from work done by the fluctuating part of the Stokes force. If $\dot{W}_\beta^P$ is computed directly in the course of a simulation, term (II) can be obtained by subtraction of term (I). In a fully developed plane channel flow where the flow field and the particle concentration have reached a statistically steady state, the first term makes a contribution only in the streamwise direction. In the wall-normal and spanwise directions, only term (II) is responsible for the power transfer.

If the same Reynolds decomposition is introduced into the expression (3.5) for the power supplied to the fluid by a particle, we obtain

$$\begin{aligned}\overline{\dot{W}_\beta^f} &= -\alpha \overline{\left[(U_\beta + \tilde{u}_\beta) - (V_\beta + \tilde{v}_\beta)\right](U_\beta + \tilde{u}_\beta)} \\ &= -\alpha \left[\underbrace{(U_\beta - V_\beta)U_\beta}_{\mathrm{I}} + \underbrace{\overline{(U_\beta - V_\beta)\tilde{u}_\beta} + \overline{(\tilde{u}_\beta - \tilde{v}_\beta)U_\beta}}_{=0} + \underbrace{\overline{(\tilde{u}_\beta - \tilde{v}_\beta)\tilde{u}_\beta}}_{\mathrm{II}} \right]. \end{aligned} \tag{3.8}$$

This expression can be interpreted in the same manner as (3.7).

The conditionally averaged particle-induced dissipation can now be obtained either by introduction of the Reynolds decomposition in (3.6) or simply by adding $\overline{\dot{W}_\beta^f}$ and $\overline{\dot{W}_\beta^P}$. In any case we find that

$$\overline{\varepsilon_\beta^P} = -\left(\overline{\dot{W}_\beta^f} + \overline{\dot{W}_\beta^P}\right) = \alpha \left[\underbrace{(U_\beta - V_\beta)(U_\beta - V_\beta)}_{\mathrm{I}} + \underbrace{\overline{(\tilde{u}_\beta - \tilde{v}_\beta)(\tilde{u}_\beta - \tilde{v}_\beta)}}_{\mathrm{II}} \right] \geqslant 0. \tag{3.9}$$

This expression shows that both the mean and fluctuating parts of the slip velocity contribute to the energy dissipation. Moreover, the slip velocity in all three coordinate directions contributes to the total mean dissipation, i.e.

$$\overline{\varepsilon^P} = \overline{\varepsilon_x^P} + \overline{\varepsilon_y^P} + \overline{\varepsilon_z^P} = \alpha \left[\underbrace{(\boldsymbol{U} - \boldsymbol{V}) \cdot (\boldsymbol{U} - \boldsymbol{V})}_{\mathrm{I}} + \underbrace{\overline{(\tilde{\boldsymbol{u}} - \tilde{\boldsymbol{v}}) \cdot (\tilde{\boldsymbol{u}} - \tilde{\boldsymbol{v}})}}_{\mathrm{II}} \right]. \tag{3.10}$$

Let us emphasize that all equations in this section are valid for a single particle. Equations (3.1)–(3.6) are instantaneous expressions, whereas (3.7)–(3.10) are conditionally averaged versions of the same and thus express mean values of the power transferred, e.g. $\overline{\dot{W}_\beta^f}$, and energy dissipated, e.g. $\overline{\varepsilon_\beta^P}$, by one single particle.

The mean power $\overline{\dot{W}_\beta^f}$ supplied by a single particle to the fluid arises from the covariance between the instantaneous slip velocity and the instantaneous fluid velocity, whereas the stress production tensor B_{ij} due to fluid–particle interactions in the Reynolds stress balance equation (2.2) originates from the covariance between the slip velocity fluctuations and the fluctuating fluid velocity. The most important distinction

Case	N_p	Φ_P	τ^+	D	a^+
A	10^5	2.9×10^{-5}	30	1041	0.36
B	10^6	2.9×10^{-4}	30	1041	0.36
C	4×10^6	0.93×10^{-3}	30	1041	0.36
D	5×10^6	1.16×10^{-3}	5	174	0.36
E	5×10^6	1.16×10^{-3}	50	1736	0.36

TABLE 1. Particle properties in five different simulations with $Re_\tau = 360$. N_p is the number of particles, Φ_P is the volume fraction and the superscript + refers to normalization with viscous units. Some primary statistics deduced from case C were presented by Zhao *et al.* (2010).

between $\overline{\dot{W}^f_\beta}$ and the corresponding diagonal component $B_{\beta\beta}$ is that the latter accounts for the reaction force from all particles in a given grid volume (see (2.7)), and therefore becomes strongly dependent on the local particle concentration.

4. Computer simulations

Five sets of particles with different numbers of particles and different particle response times were simulated in fully developed turbulent channel flow at a friction Reynolds number $Re_\tau = 360$ based on the distance h between the two parallel walls. An overview of the five cases is given in table 1. Here, and in the rest of this paper, the superscript + denotes normalization with the viscous scales for length ν/u_τ and time ν/u_τ^2. Since we are concerned only with dilute particle suspensions in which particle–particle collisions are rare and can be neglected, the overall volume fraction Φ_P was $\sim 10^{-3}$ or lower.

The size of the computational domain was $6h$ and $3h$ in the streamwise x-direction and the spanwise z-direction, respectively. The Navier–Stokes equation (2.1) for particle-laden flows was discretized on 128^3 grid nodes. Periodic boundary conditions were imposed in the two homogeneous directions and no-slip and impermeability boundary conditions were enforced at the solid channel walls ($y = 0$ and $y = h$). The DNS-solver is the same as that used by Gillissen *et al.* (2008), Zhao *et al.* (2010) and Zhao & Andersson (2011). A pseudospectral method using Fourier series in the two homogeneous directions and a second-order finite-difference scheme in the wall-normal direction is employed for the spatial derivatives on a staggered grid system. The time advancement is carried out with a second-order explicit Adams–Bashforth scheme.

In all the five cases the particles were released randomly in an already fully developed turbulent channel flow, and statistics were not gathered until a sufficient level of steadiness had been achieved. Although the particles were introduced evenly throughout the flow field, the particles tend to drift towards the walls, as shown by the particle concentration profile in figure 1 deduced from case C. The particle concentration is therefore substantially higher in the near-wall region than in the core of the channel. Moreover, the particles are not distributed homogeneously even at a given wall distance. The tendency of inertial particles to concentrate preferentially has been addressed for instance by Eaton & Fessler (1994). Figure 2 shows an instantaneous particle distribution in an (X, Z)-plane in the so-called buffer region, where the flow field is characterized by elongated low-speed streaks. In localized areas

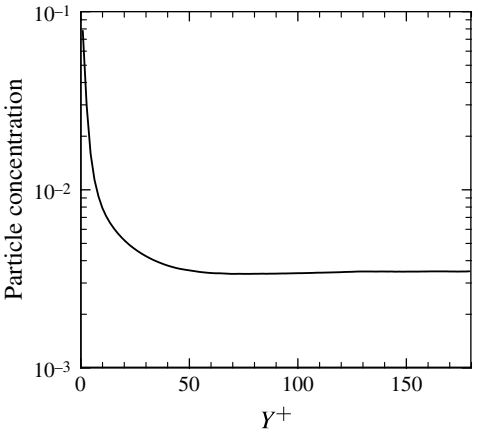

FIGURE 1. Particle concentration profile of case C (ratio of the local number of particles to the total number of particles) in the wall-normal direction.

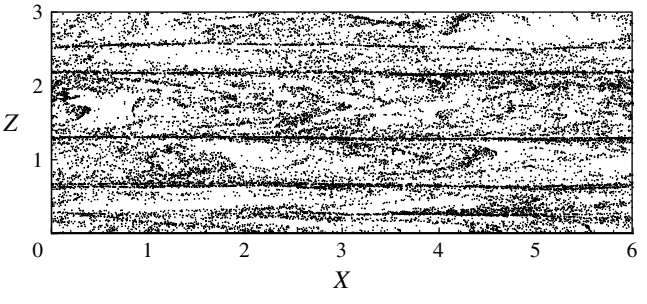

FIGURE 2. Instantaneous particle distribution of case C in the X–Z plane at $Y^+ \approx 18$.

in the near-wall region, the particle concentration may therefore occasionally exceed the limit beyond which particle–particle collisions will occur.

Some of the statistical results which will be presented in § 6 of this paper were obtained by conditional sampling rather than by conventional Reynolds-averaging. Conditional sampling has been used before in one-way coupled simulations, for instance by Squires & Eaton (1990), Mortensen *et al.* (2007, 2008) and Zhao, Marchioli & Andersson (2012). The fluid velocity of interest is that at the particle positions, since only that velocity is involved in the Stokes drag force in (2.5). Inertial particles tend to concentrate in preferred areas where the local fluid velocity differs significantly from the Reynolds-averaged fluid velocity, and conditional sampling is therefore crucially important.

5. Effects of particle response time and loadings

Statistical results from cases A–C, i.e. with three different particle loadings, will be compared in order to demonstrate the importance of the loading on the modulation of the turbulence. Furthermore, cases C–E with different particle response times but similar volume fractions were designed to investigate how the particle response time

influences the turbulent flow. These parameter studies are presented in §§ 5.1 and 5.2, respectively.

5.1. *The effect of particle volume fraction*

It can readily be observed from figure 3 that the fluid flow field and the turbulence statistics are practically unaffected by the presence of the solid particles in case A with modest particle loading. The data are almost indistinguishable from the results of the unladen channel flow simulation (denoted by symbols). This is consistent with earlier observations by Picciotto *et al.* (2006) from a simulation with the same number of particles. In cases B and C, both with substantially higher loadings of the same particles, the mean fluid velocity has increased in spite of the constant driving pressure gradient. Some primary results from case C were presented by Zhao *et al.* (2010), who emphasized that the enhanced mean flow is equivalent to drag reduction. This is in accordance with the laboratory measurements by Rossetti & Pfeffer (1972). The turbulence field has also been severely affected. The streamwise turbulence intensity is augmented whereas the velocity fluctuations in the spanwise and wall-normal directions have been damped, along with substantial attenuation of the Reynolds shear stress in figure 3(*f*). It is noteworthy that only modest changes are observed when the number of particles is increased from 0.1×10^6 to 1.0×10^6, whereas major changes occur when the N_P is further increased to 4×10^6.

5.2. *The effect of particle response time*

The effect of the particle response time τ^+ is shown in figure 4. Results from the three particle sets of cases C–E with different τ^+-values are compared with statistics from an unladen channel flow. Firstly, an interesting finding is that the modulations of the turbulence field by the solid particles are selectively dependent on the particle response time. In case D with the modest response time $\tau^+ = 5$ no noticeable changes are observed in the mean streamwise velocity profile and the streamwise turbulence intensity, even though the particle volume fraction is almost as high as in cases C and E. Nevertheless, the velocity fluctuations in the spanwise and wall-normal directions are attenuated, and so is the Reynolds shear stress. Secondly, the other two sets of particles with larger inertia, i.e. cases C and E, exhibit a substantial impact of the particles on the mean velocity profile as well as on the turbulence intensities and the Reynolds shear stress. These effects are most pronounced in case E with $\tau^+ = 50$, i.e. the most inertial particles.

In one-way coupled simulations by Zhao & Andersson (2012) the particles fluctuated less vigorously than the fluid in the spanwise and wall-normal directions, whereas the streamwise agitation of the particles exceeded the streamwise turbulence intensity. With inclusion of particle–turbulence interactions in the two-way coupled simulations presented herein, the particles tend to enhance the streamwise fluid velocity fluctuations and correspondingly reduce the spanwise and wall-normal fluctuations. In case D, the modulations of the flow field occurred only in the spanwise and wall-normal directions whereas the streamwise fluctuations were left unaffected. This is because two independent mechanisms of particle–fluid interactions exist, which apparently play different roles in different directions. These two mechanisms of turbulence attenuation or augmentation will be explored in terms of transfer of kinetic energy between the particle and fluid phases and the extra energy dissipation in the following section. At this stage, however, we can conclude that the modulation of the turbulence by solid particles is (i) caused by two different mechanisms, and (ii) largely dependent on the particle inertia.

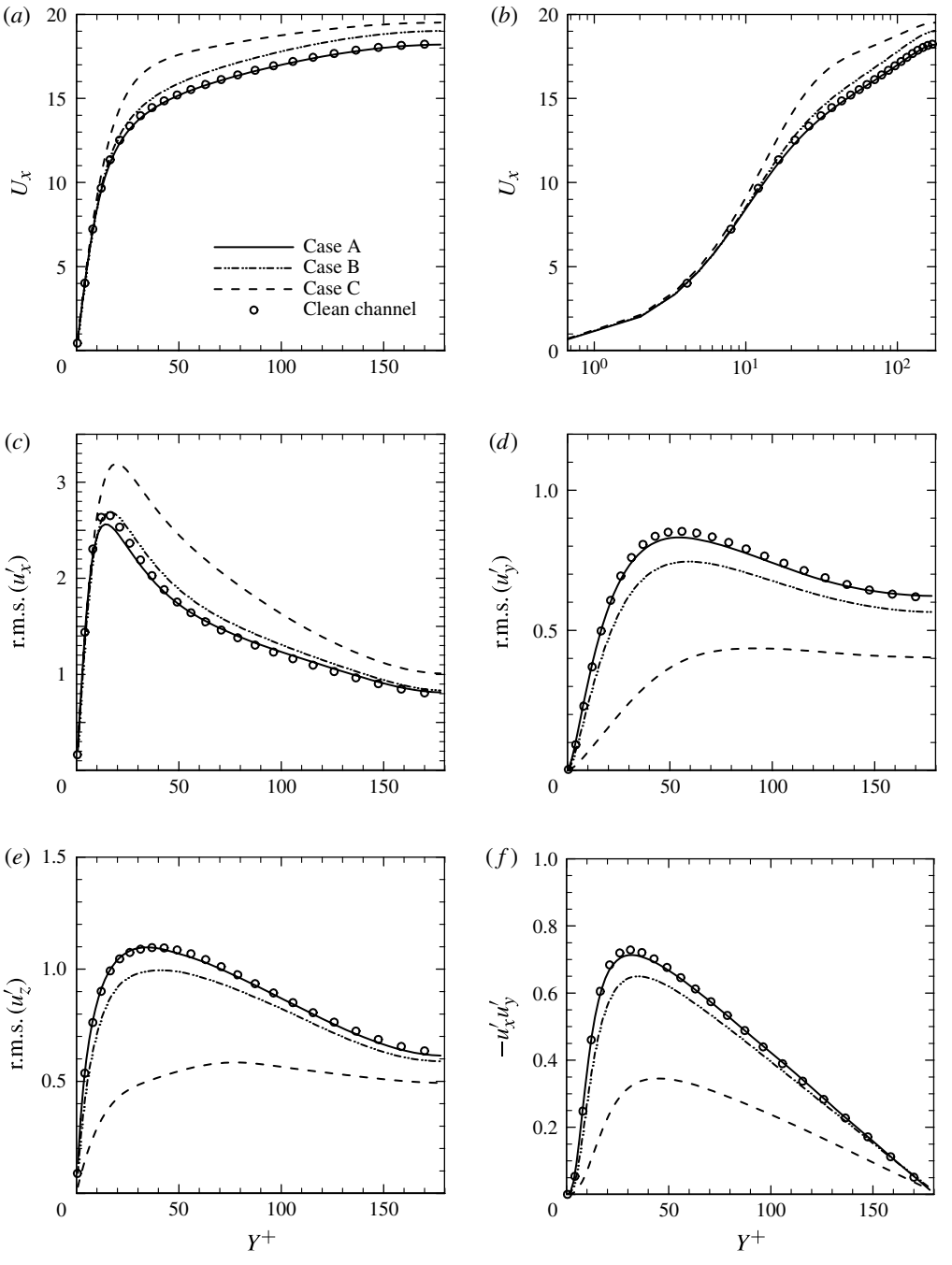

FIGURE 3. Primary fluid velocity statistics for cases A–C. Comparison between particle-free flow (symbols) and particle-laden flows (lines): (*a,b*) mean velocity in the streamwise direction with linear and semi-logarithmic scaling; (*c*) velocity fluctuations in the streamwise direction; (*d*) velocity fluctuations in the wall-normal direction; (*e*) velocity fluctuations in the spanwise direction; (*f*) Reynolds shear stress.

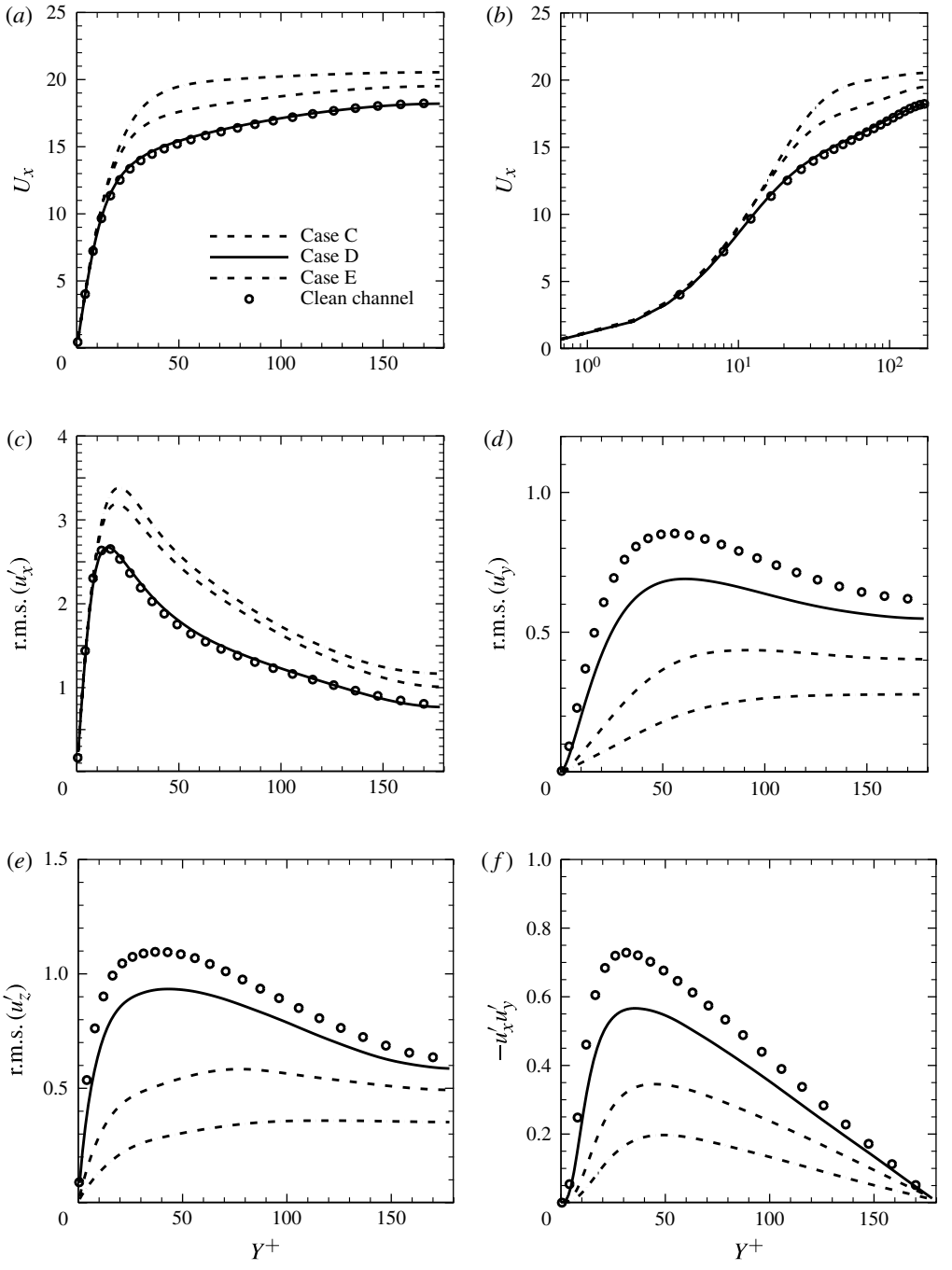

FIGURE 4. Primary fluid velocity statistics for cases C–E. Comparison between particle-free flow (symbols) and particle-laden flows (lines): (*a,b*) mean velocity in the streamwise direction; (*c*) velocity fluctuations in the streamwise direction; (*d*) velocity fluctuations in the wall-normal direction; (*e*) velocity fluctuations in the spanwise direction; (*f*) Reynolds shear stress.

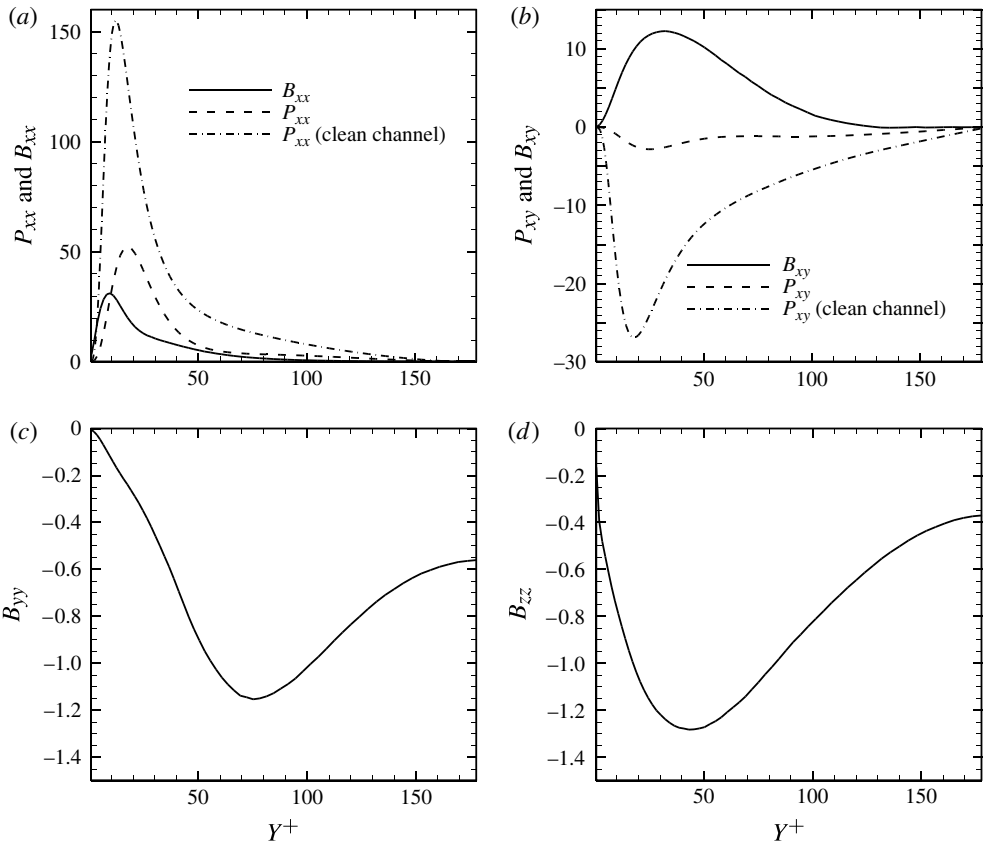

FIGURE 5. Production terms P_{ij} and B_{ij} in the Reynolds stress budgets: (*a*) B_{xx} and P_{xx} compared with P_{xx} in the clean channel flow; (*b*) B_{xy} and P_{xy} compared with P_{xy} in the clean channel flow; (*c*) profile of B_{yy} and (*d*) B_{zz}.

6. Modulations in flow structure and kinetic energy transfer

Primary Reynolds-averaged statistics which showed the influence of particle loading and particle response time on the turbulence modulation were presented in § 5. To obtain further insight into the complex fluid–particle interactions, the typical case C is further investigated with a view to explaining the mechanisms of the turbulence modulations. Firstly the production terms due to mean shear and the body force terms due to the presence of particles will be presented in § 6.1. Secondly the turbulence modulations are analysed in terms of the kinetic energy transfer between fluid and particles in § 6.2. Finally, scatter plots are introduced in § 6.3 as an effective means of pinpointing the influence of the slip velocity on the kinetic energy transfer and energy dissipation.

6.1. *The production and particle terms in the Reynolds stress budgets*

In a fully developed plane channel flow, the mean shear production tensor P_{ij} has zero diagonal elements in the spanwise and wall-normal directions. All the non-zero production terms are shown in figure 5. One can first of all observe that both $B_{yy} = 2\overline{\tilde{u}_y \tilde{f}_y^p}$ and $B_{zz} = 2\overline{\tilde{u}_z \tilde{f}_z^p}$ are negative across the entire channel. Since

the corresponding mean shear production terms P_{yy} and P_{zz} are zero, the negative production due to the fluid–particle interactions offers a reasonable explanation for the significant reduction of $\overline{\tilde{u}_y\tilde{u}_y}$ and $\overline{\tilde{u}_z\tilde{u}_z}$. Admittedly, the observations that B_{yy} and B_{zz} are negative and thus act as sink terms in their respective budget equations do not necessarily translate to a change of the corresponding Reynolds stress component. In a general situation the appearance of an extra sink term in (2.2) tends to reduce the rate of change of the actual stress component. If the left-hand side of (2.2) vanishes, as in the present situation of a statistically steady and fully developed channel flow, a sink term which arises on the right-hand side is likely to reduce the Reynolds stress component of interest.

In the lower half of the plane channel $P_{xy} < 0$, whereas $B_{xy} = \overline{\tilde{u}_x\tilde{f}_y^P} + \overline{\tilde{u}_y\tilde{f}_x^P} > 0$. The fluid–particle interactions therefore tend to oppose the mean shear production and thereby reduce the magnitude of $\overline{\tilde{u}_x\tilde{u}_y}$. This is indeed what we have already observed.

Finally, the second moments $\overline{\tilde{u}_x\tilde{u}_x}$ are produced both by means of mean flow Reynolds-stress interactions $P_{xx} > 0$, and particle–fluid interactions $B_{xx} = 2\overline{\tilde{u}_x\tilde{f}_x^P} > 0$. However, a closer look at figure 5(*a*) shows that, in spite of the extra positive production B_{xx}, the total production $P_{xx} + B_{xx}$ is slightly reduced in the particle-laden flow as compared to the unladen channel flow. Nevertheless, the streamwise turbulence intensity is substantially enhanced: see e.g. figure 4(*c*). The higher $\overline{\tilde{u}_x\tilde{u}_x}$ in the particle-laden flow may possibly be due to a reduction of the viscous dissipation ε_{xx} in the presence of particle additives, which more than outweighs the modest decrease in total production.

The analysis above was limited to examinations of the alterations in the mean shear production P_{ij} and the particle terms B_{ij} due to the solid particles. These terms are believed to play dominating roles in the Reynolds stress budgets (2.2). However, it is likely that the presence of inertial particles in the flow will also affect the pressure–strain interactions, the viscous energy dissipation, and the turbulent diffusion (i.e. the triple velocity correlations). An investigation of these effects is beyond the scope of the present study.

6.2. *Kinetic energy transfer between particles and fluid*

To get a first impression of the particle-laden flow some contour plots are shown in figure 6. A snapshot of the modulated turbulence field, as reported by Zhao *et al.* (2010), is depicted in figure 6(*a*). The typical smaller-scale eddies close to the walls have been damped, and point particles are clustering in preferred regions while other zones are void. It is immediately observed that both the fluid and particle streamwise velocities, i.e. u_x and v_x, are positive throughout the entire cross-section in figures 6(*a*) and 6(*b*), respectively. From the different quadrants in (3.3) we can infer that the fluid exerts work on the particles when the Stokes force is positive, i.e. in the red zones in figure 6(*c*), and $\dot{W}_x^P < 0$ in the blue zones. Negative values of the Stokes force occur almost solely in the close vicinity of the channel walls, whereas contours of a positive drag force can be observed far away from the wall and even in the channel centre. We therefore believe that the point particles tend to absorb kinetic energy from the large-scale eddies in the core region of the channel and transfer the energy back to the smaller-scale eddies adjacent to the walls. This interpretation is consistent with the force statistics which is to be presented in figures 8 and 9.

Another noteworthy observation that can be made from figure 6 is that particularly high positive values of $-f_x^p$ are associated with strong ejections of low-speed fluid away from the walls. Strong ejections from the lower wall are seen at $Z \approx 0.45, 1.0$

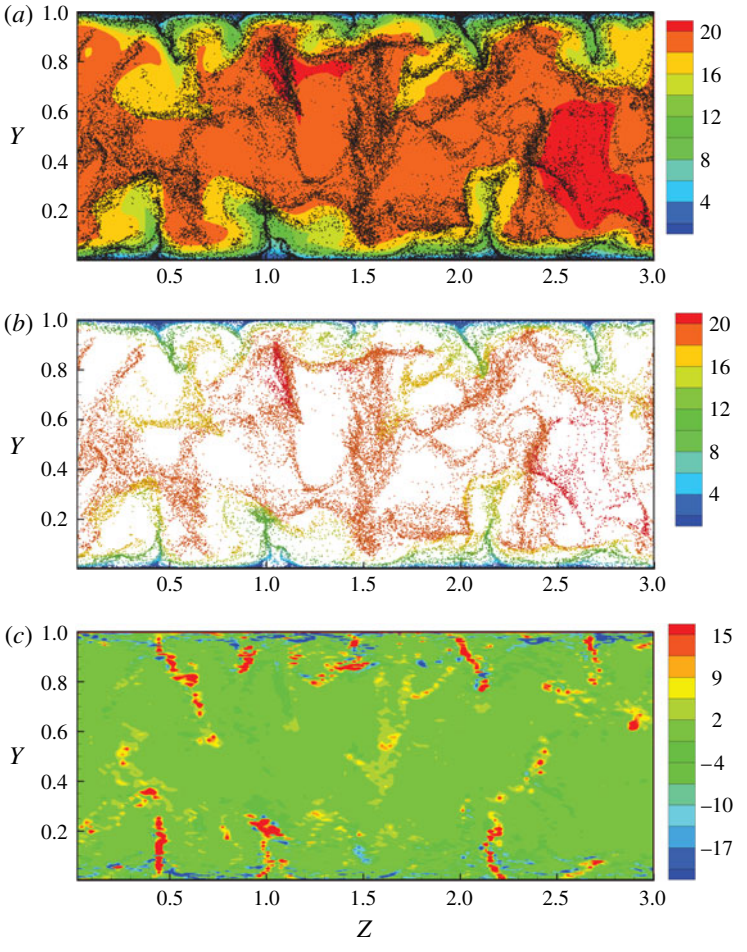

FIGURE 6. Instantaneous flow contours in a cross-sectional (y, z)-plane: (a) streamwise fluid velocity u_x (colour contours) and point particle distribution (black dots); (b) streamwise particle velocity v_x; (c) streamwise component of the drag force $-f_x^p$ from the fluid on the particles.

and 2.2 and from the upper wall at $Z \approx 0.4, 2.1$ and 2.7. According to (3.6) the particle dissipation ε_P is proportional to the square of the magnitude of the Stokes force. High energy dissipation rates are therefore associated with the ejection events. In this regard, one should recall that Rashidi *et al.* (1990) observed experimentally that the number of ejections was reduced in the presence of small polystyrene particle additives as compared with the unladen flow. The turbulence intensities and the Reynolds shear stress were correspondingly damped. The particularly high energy dissipation rate associated with the ejections might explain why the number of ejections is reduced.

In wall-bounded turbulence particles are carried towards the wall during sweeping events and lifted away from the wall by the ejections. The contour plots in figure 7 show the fluid and particle velocities and the Stokes drag force in the wall-normal direction at exactly the same instant in time as for the contour plots in figure 6. Figure 7(b) confirms that $v_y > 0$ around the ejections from the lower wall observed in

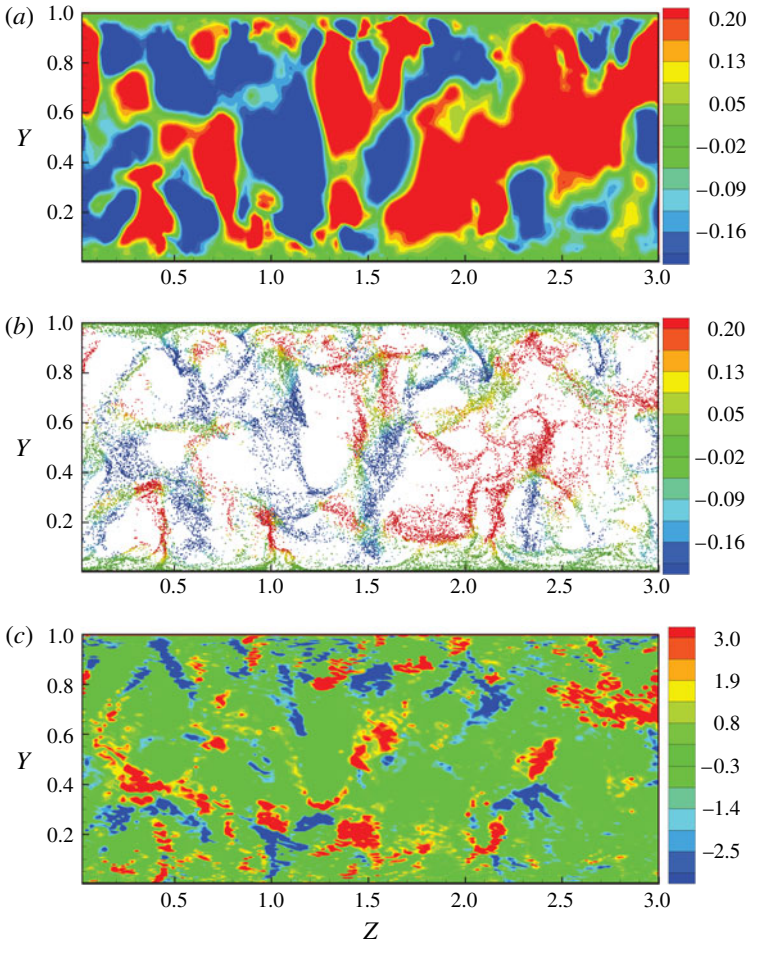

FIGURE 7. Instantaneous flow contours in a cross-sectional (y, z)-plane at the same time instant as in figure 6: (*a*) wall-normal fluid velocity u_y (colour contours); (*b*) wall-normal particle velocity v_y; (*c*) wall-normal component of the drag force $-f_y^p$ from the fluid on the particles.

figure 6(*b*), whereas v_y attains negative values near the locations where fluid is ejected away (i.e. downwards) from the upper wall. However, the direction of the wall-normal drag force displayed in figure 7(*c*) is not uniquely related to the direction of the local flow. The particle motion away from the wall along with the ejection events is apparently driven by Stokes drag in most cases. However, such a covariance between the direction of the Stokes force and the particle motion is not observed around the distinct ejection event close to $Z = 1$ at the lower wall.

The mean values of the drag force acting from the fluid on the particles are shown in figure 8. The Stokes drag force F_i on individual point particles given in (2.5) is first summed up for all particles in a given grid cell, as in (2.7), and thereafter averaged in time and in the two homogeneous coordinate directions. The streamwise component $-\overline{f_x^p}$ is positive and fairly uniform from $Y^+ > 50$ and all the way to the channel centre. This is consistent with the contour plot in figure 6(*c*), where significant

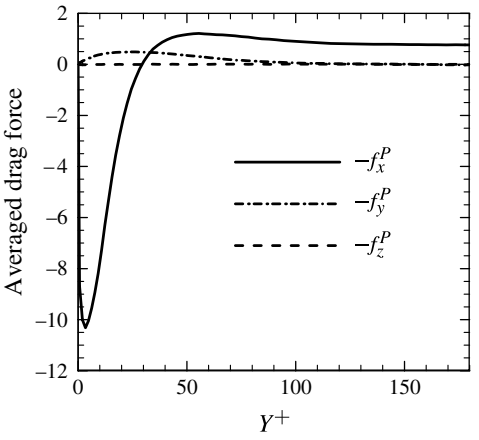

FIGURE 8. Profiles of the directional components of the averaged drag force $-\overline{f_i^P}$.

negative force values were observed only in the vicinity of the walls. Indeed, the $-\overline{f_x^P}$ profile in figure 8 changes sign at $Y^+ \approx 36$ and attains large negative values in the buffer layer and the viscous sublayer, with a distinct negative peak at about $Y^+ \approx 4$. The pronounced negative values of the mean Stokes force reflect that the mean particle velocity $\overline{V_x}$ exceeds the mean fluid velocity $\overline{U_x}$ at the particle positions. One should recall, however, that the fluid velocity seen by the particles is lower than the Reynolds-averaged fluid velocity since the inertial particles tend to concentrate in regions with locally low fluid velocity in the streamwise direction. Due to the particle inertia, the particles do not adjust to local flow conditions but retain their higher streamwise momentum. In the logarithmic layer and further out, however, the particles lag the local fluid velocity, as observed for instance in the experiments by Rashidi *et al.* (1990).

The wall-normal component $-\overline{f_y^P}$ appears to be modestly positive in the near-wall region but becomes vanishingly small in the core region of the channel. The mean Stokes force is therefore directed away from the lower wall and thus opposes the slow drift of particles towards the wall (Zhao *et al.* 2012). This so-called turbophoresis is known to be responsible for the tendency of inertial particles to accumulate in the near-wall region, as shown in figure 1. This phenomenon vanishes when the particle concentration has reached a statistically steady state. According to the $-\overline{f_y^P}$ profile in figure 8, the turbophoresis effect is not caused by the Stokes drag in the wall-normal direction. To the contrary we believe that $-\overline{f_y^P} > 0$ tends to reduce the number of particle collisions with the wall. It should be pointed out that $-\overline{f_y^P}$ exhibits an anti-symmetric variation across the channel, i.e. the wall-normal Stokes drag is directed away from the wall on both sides of the channel. The mean Stokes drag in the spanwise direction, on the other hand, turns out to be vanishingly small in figure 8. This is due to the symmetry properties of the present flow problem and the observation that $-\overline{f_z^P} \approx 0$ signifies the adequacy of the present sampling.

The only feedback from the point particles on the fluid motion is through the instantaneous force $\boldsymbol{f}^P$ in (2.1). This force represents the cumulative reaction on the fluid from a finite number n_p of point particles in a given fluid element or grid cell, in accordance with (2.7). The results presented so far are therefore crucially dependent on the local particle concentration.

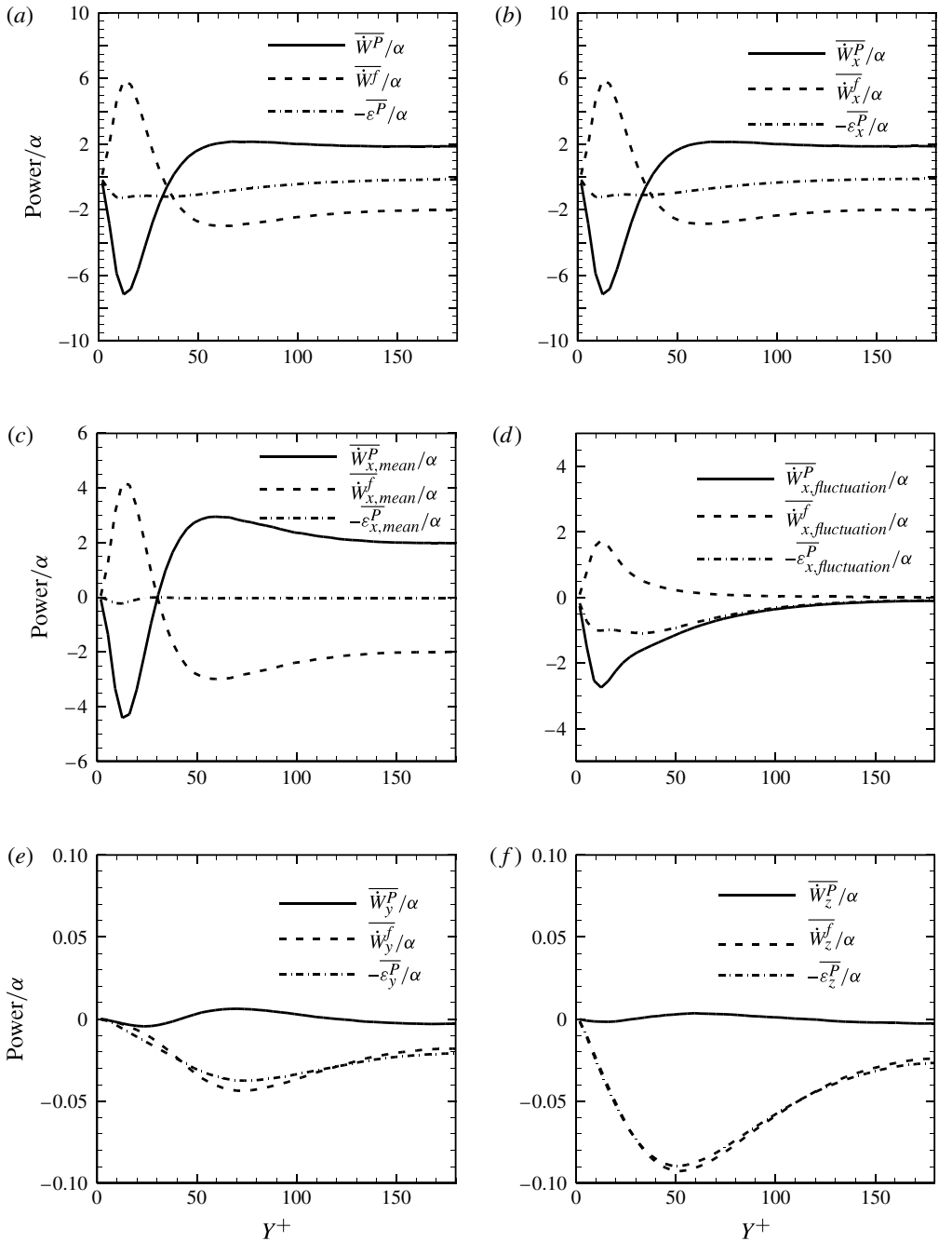

FIGURE 9. Profiles of the mean power transferred from the fluid to a single particle $\overline{\dot{W}^P}$, from the particle to the fluid $\overline{\dot{W}^f}$ and the particle dissipation $\overline{\varepsilon^P}$: (*a*) accumulated results; (*b*) overall data in the streamwise direction; (*c*) contributions from the mean velocities in the streamwise direction; (*d*) contributions from the velocity fluctuations in the streamwise direction; (*e*) contributions from the velocity fluctuations in the wall-normal direction; (*f*) contributions from the velocity fluctuations in the spanwise direction.

Let us proceed and examine the exchange of mechanical energy between the fluid and a single particle on the basis of the theoretical analysis in § 3. The point force $\boldsymbol{F}$ in (2.5) is essential for the instantaneous power exchange between the fluid and a particle in (3.2) and (3.5) and in the particle-induced energy dissipation in (3.6). Now conditional averages of the power exchange and energy dissipation rate defined in (3.7)–(3.10) are presented. These statistics are average values for a single particle located at a given distance from the wall. The energy transfer and dissipation are shown in figure 9(*a*), with the directional contributions detailed in the subsequent panels in order to give us further insight into the transfer processes.

The overall energy transfer rates are evidenced by the profiles in figure 9(*a*). Roughly opposite trends are observed for $\overline{\dot{W}^P}$ and $\overline{\dot{W}^f}$. The particles exert work on the local fluid in the buffer layer and viscous layer ($\overline{\dot{W}^P} < 0$ and $\overline{\dot{W}^f} > 0$) whereas the particles receive energy from the fluid ($\overline{\dot{W}^P} > 0$ and $\overline{\dot{W}^f} < 0$) beyond $Y^+ \approx 36$. During a transient stage in which the particles drift slowly towards the wall (not considered here), one may argue that the particles represent a vehicle for energy transport away from the core region. On average, the particles receive energy from the fluid in the centre region and return most of the energy back to the fluid in the near-wall region.

A particularly noteworthy observation which can be made from figure 9(*a*) is that $\overline{\dot{W}^P}$ and $\overline{\dot{W}^f}$ do not add up to zero but to a non-zero $-\overline{\varepsilon^P}$. The imbalance between the power transferred from the fluid to the particle ($\overline{\dot{W}^P}$) and the power received by the fluid from the particle ($\overline{\dot{W}^f}$) is a measure of the extra energy dissipation caused by the point particle. The particle dissipation is most pronounced in the near-wall region but retain an appreciable level also in the inner part of the logarithmic layer. Thus $\overline{\varepsilon^P}$ can be considered as a scalar measure of the particle–turbulence interactions, which are indeed most profound in the vicinity of the wall where the highest particle density is also found.

In an attempt to explain the modulations of the turbulence field observed in figures 3 and 4, the Reynolds decomposition is introduced into $\dot{W}^P_\beta$ and $\dot{W}^f_\beta$ defined in (3.2) and (3.5), respectively. We then arrive at (3.7) and (3.8), which show that both the mean velocities and the velocity fluctuations contribute to the energy exchange process. Furthermore, care is taken to distinguish between the contributions from different directional components of the velocity vectors. Firstly, the total power associated with the streamwise motions is shown in figure 9(*b*). The profiles in this panel are almost indistinguishable from the corresponding distributions in figure 9(*a*). It is therefore tempting to conjecture that almost all the energy exchange between the two phases is associated with the streamwise motions. The distinct positive peak of $\overline{\dot{W}^f_x}$ in the near-wall region is probably associated with enhancement of the fluid turbulence intensity in the streamwise direction seen in figure 3(*c*).

We proceed to see whether the mean motion or the velocity fluctuations are the most dominant. Examination of the contributions from the mean in figure 9(*c*) and from the fluctuations in figure 9(*d*) reveals a number of important findings. The profiles in figure 9(*c*) are surprisingly similar to the profiles in figure 9(*b*), although the characteristic near-wall peak values are about 50 % higher in figure 9(*b*) than in figure 9(*c*). The profiles shown in figure 9(*d*) confirm that this excess power exchange in the near-wall region is contributed by the velocity fluctuations. However, the substantial contributions from the streamwise fluctuations decay monotonically towards the channel centre where almost all the energy exchange stems from the mean velocities. It is noteworthy that the contributions from the fluctuating velocity field

give rise to a consistently negative $\overline{\dot{W}_x^P}$ and a positive $\overline{\dot{W}_x^f}$ all the way from the wall to the channel centre. The average energy transfer caused by the streamwise velocity fluctuations are thus from the particles to the fluid, irrespective of the distance from the wall.

Although the energy exchange between the two phases due to the mean motion exceeds the exchange caused by the velocity fluctuations, the particle dissipation $\overline{\varepsilon^P}$ associated with the latter is at least five times greater than the dissipation caused by the mean motions. This somewhat surprising observation is a direct consequence of the recent finding by Zhao *et al.* (2012) that the fluctuating part of the slip velocity vector is more energetic than the corresponding mean slip velocity. Thus, the energy associated with the particle fluctuations is partly given away to the fluid and partly being dissipated.

In order to complete the detailed exploration of the energy transfer and dissipation mechanisms, the contributions associated with wall-normal and spanwise velocity fluctuations are shown in figures 9(*e*) and 9(*f*), respectively. In both panels, the power received by the fluid from the particle dominates, and reaches a negative minimum value around $Y^+ \approx 50$–60. The negative values of $\overline{\dot{W}_y^f}$ and $\overline{\dot{W}_z^f}$ imply that work done by a particle on the local fluid is negative. Since the energy transfer from the fluid to the particles is of marginal importance, we obtain from (3.9) that $\overline{\varepsilon_y^P} \approx -\overline{\dot{W}_y^f}$ and $\overline{\varepsilon_z^P} \approx -\overline{\dot{W}_z^f}$. This leads to the conclusion that, as far as motions in the cross-sectional plane are concerned, energy is drained from the fluid motion and dissipated rather than transferred to the particle motion.

The fluid motions in the (y, z)-plane appear to be unable to exert work on the particles. According to (3.2), this implies that the covariance of the particle and fluid velocity fluctuations is almost equal to the particle intensity in that direction. This does not necessarily imply that the covariance also equals the fluid intensity. Indeed, we observed that $\overline{\dot{W}_y^f}$ attains an appreciable level although $\overline{\dot{W}_y^P} \approx 0$. This observation is an outcome of particle inertia. The particles are unable to follow the eddy motion in the cross-sectional plane and the unresponsive particles give rise to extra dissipation, which in turn plays a crucial role in the attenuation of the wall-normal and spanwise turbulence intensities shown in figure 3(*d,e*).

Let us finally emphasize that the contributions to the energy exchange and dissipation from the streamwise motions dominate over the contributions from the motions in the cross-sectional plane. The latter is, however, by no means negligible, and tends to explain the observed modulations of the turbulence field in figure 3. In particular, the enhancement of the streamwise fluctuations in the near-wall region arises partly due to work associated with the mean motion and partly due to work related to the velocity fluctuations. The attenuation of the spanwise and wall-normal motion is, on the other hand, caused by particle-induced energy dissipation.

The mean streamwise fluid velocity in figure 10(*a*) is strikingly different from the Reynolds-averaged mean velocity. While the particle mean velocity is consistently lower than the Reynolds-averaged fluid velocity, the particle velocity exceeds the conditionally averaged fluid velocity in the buffer region and lags the fluid velocity seen by the particles in the core region. As far as the root mean square (r.m.s.) values of the velocity fluctuations are concerned, i.e. the directional intensities, the particle intensities are substantially closer to the conditionally averaged fluid intensities than to the fluid intensities obtained by conventional Reynolds-averaging. Similar observations were made by Mortensen *et al.* (2008) in one-way coupled simulations. These findings

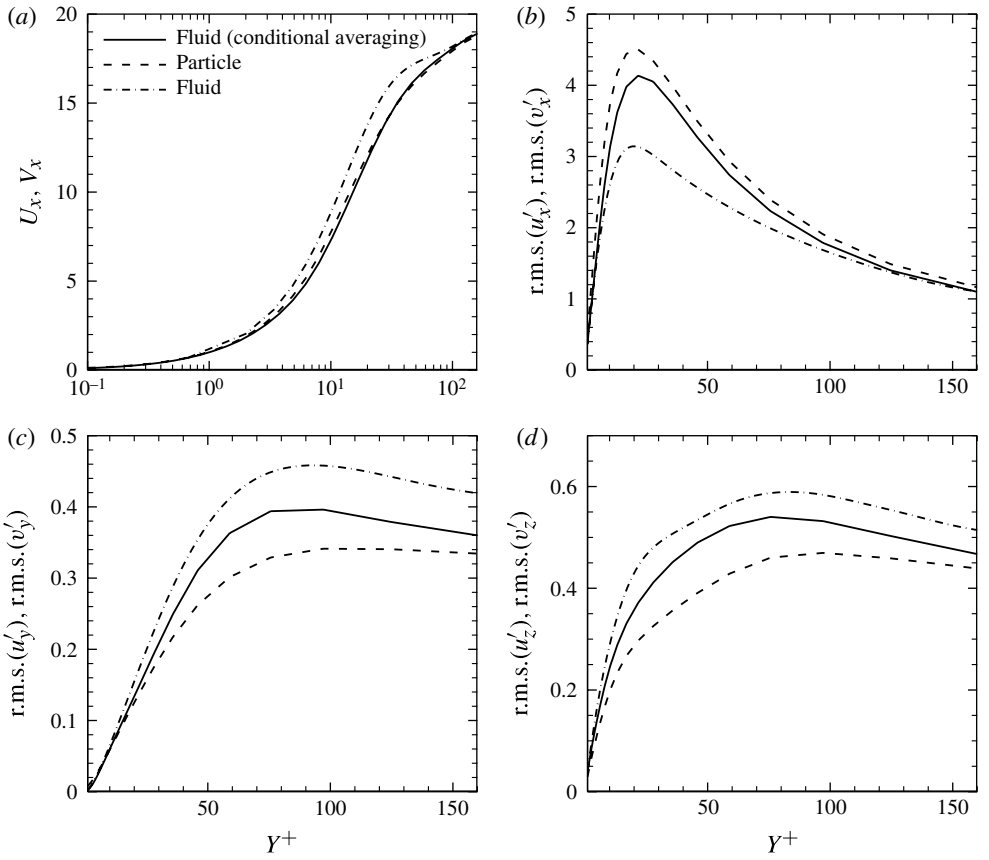

FIGURE 10. Comparison between traditionally sampled fluid statistics and conditionally sampled results on the particle positions: (*a*) streamwise mean velocity; (*b*) streamwise velocity fluctuations; (*c*) wall-normal velocity fluctuations; (*d*) spanwise velocity fluctuations.

are, however, of particular relevance in the present study since the slip velocity plays a crucial role in the interphasial energy transfer discussed in § 3.

The directional energy spectra at three different distances from the wall shown in figure 11 aim to reveal whether the effect of the particle additives is concentrated at particular length scales. As far as the motion in the cross-sectional plane is concerned, the damping of the fluid motion prevails across the entire range of scales. Around the wall region, e.g. at $Y^+ = 7$, all scales of turbulence are damped due to the particles as compared with the unladen flow. In the centre of the channel, the streamwise fluctuations, which are enhanced by the inertial particles, appear to be damped at smaller scales and only the largest eddies become more energetic. In spite of the particles being point particles, even the large-eddy motion is severely affected by the presence of the particles.

In the critical buffer layer at $Y^+ = 19$ the spectra in figure 11(*b*) show that the turbulence has been damped by the presence of the inertial particles. Instantaneous contour plots of the streamwise velocity component at $Y^+ = 20$ presented by Zhao *et al.* (2010) showed that the small scales had been damped in the particle-laden flow, whereas the streamwise coherence of the near-wall flow structures was considerably

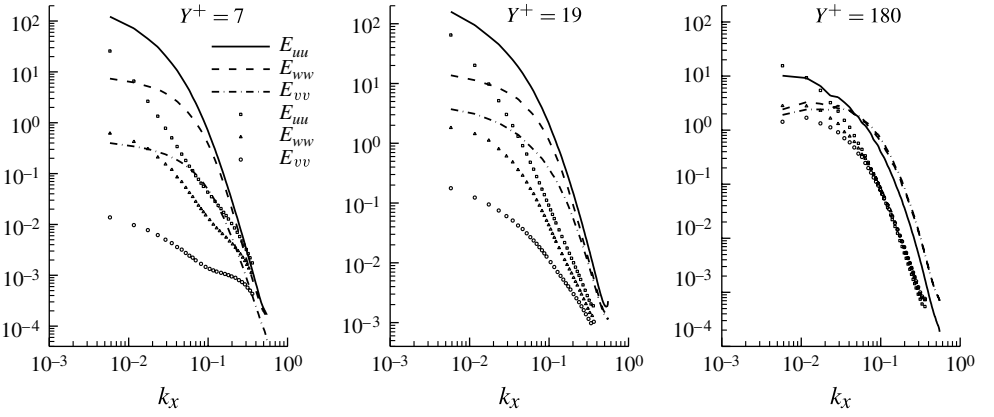

FIGURE 11. One-dimensional spectra of the fluid kinetic energy in three different planes: lines, unladen channel flow; symbols, particle-laden flow of case C.

increased and the alternating high- and low-velocity streaks appeared to be wider and more regular than in the unladen flow. The spectra in figure 11(*b*) thus confirm that the turbulence has indeed been damped whereas fairly energetic coherent streaks persist.

The present study shows that the presence of solid particles may lead to drag reduction, even though the particles are tiny spheres and not elongated fibre-like particles or elastic polymers, for which drag reduction is a well-established phenomenon (e.g. Gillissen *et al.* 2008). It should be recalled that the present flow was driven by a given streamwise mean pressure gradient and we could observe from figure 3(*a*) that the bulk flow increased when the particles were added to the flow. The increased bulk flow for a given pressure gradient is deemed to be equivalent to drag reduction (i.e. pressure-loss reduction) if the bulk flow is given. The drag reduction for case C particles has been reported by Zhao *et al.* (2010).

Only a modest number of papers have convincingly reported observations of drag reduction achieved by means of spherical particles. Rossetti & Pfeffer (1972) performed measurements in vertical and horizontal channel flows of dilute suspensions of glass beads and reported drag reduction at Reynolds numbers in the range from 10 000 to 25 000 with different mass loadings. Li *et al.* (2001) and Yamamoto *et al.* (2001) performed LES and DNS of particle-laden flow in a vertical channel with gravity included, in order to compare their results with the experimental measurements by Kulick *et al.* (1994). They both observed an increase of the mean streamwise velocity for mass loadings 1 and 0.4. The modulations they reported in the turbulence field are in qualitative accordance with the present results. Yamamoto *et al.* (2001), however, argued that the drag reduction observed could be ascribed to the presence of the gravity force, which tends to accelerate the local fluid. In the present study, on the other hand, gravity has been ignored and an increased bulk flow is nevertheless observed. It can therefore be concluded that gravity is not the only means by which drag reduction can be achieved, and other mechanisms do exist. The present investigation may serve the purpose of elucidating these mechanisms.

6.3. *Analysis of kinetic energy transfer by scatter plots*

In two-way coupled simulations of particle-laden flows, mechanical energy is continuously exchanged between the fluid and particle phases. Moreover, a fraction

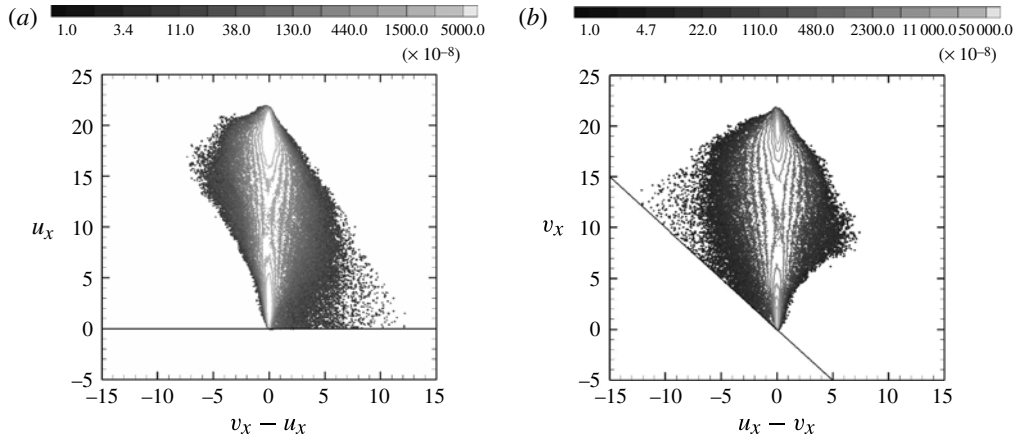

FIGURE 12. Scatter plot of streamwise velocity components: (*a*) fluid velocity versus slip velocity; (*b*) particle velocity versus slip velocity. The straight lines in (*a,b*) are $u_x = 0$ and $v_x = -(u_x - v_x)$, respectively.

of the mechanical energy is lost during the exchange process, and gives rise to what we call particle dissipation. According to the analysis in § 3, the interphasial energy exchange depends on the covariance between the slip velocity and the particle or fluid velocities, as shown in (3.2) and (3.5), respectively. In this subsection scatter plots between a given fluid or particle velocity component and the slip velocity component in the same direction are presented in order to further elucidate the energy exchange processes.

Instantaneous values of the streamwise fluid velocity u_x are plotted against the streamwise component of the slip velocity vector $v_x - u_x$ in figure 12(*a*). Similarly, the streamwise particle velocity v_x is shown against $u_x - v_x$ in figure 12(*b*). The plots are arranged so that contributions to positive power supply $\overline{\dot{W}_x^f}$ and $\overline{\dot{W}_x^P}$ are to the right as long as u_x and v_x never attain negative values. The colour-coding represents the density of events, i.e. the joint probability density function (p.d.f.). The p.d.f. exhibits two different peaks, both close to $u_x - v_x = 0$. Notice that the contour lines representing the very highest densities are omitted to facilitate a clear interpretation of the plots. One peak in figure 12(*a*) is around $u_x \approx 3$, i.e. in the viscous sublayer, and the other peak is slightly below $u_x = 20$ in the channel centre. The high probability of $v_x - u_x \approx 0$ in the core region shows that the inertial particles are more able to follow the fluid motion in the region where the time scale of the prevailing large-eddy motion is relatively large. The p.d.f. is severely skewed towards the right ($v_x - u_x > 0$) around the lower peak and towards the left ($v_x - u_x < 0$) around the higher peak. On average the work on the fluid by the particles gives rise to $\overline{\dot{W}_x^f} > 0$ in the viscous sublayer whereas $\overline{\dot{W}_x^f}$ becomes negative in the core region of the channel. These findings are fully consistent with the cross-sectional snapshot in figure 6(*c*) and the statistics shown in figure 9(*b*). The asymmetry of the scatter plot in figure 12(*b*) is qualitatively different and less pronounced than in figure 12(*a*). The straight line is the demarcation line between positive and negative values of u_x, and no events with $u_x < 0$ (i.e. below the line) are observed. The scatter plot is skewed towards the left for lower values of v_x and the covariance between v_x and $(u_x - v_x)$ becomes negative in the near-wall region. The

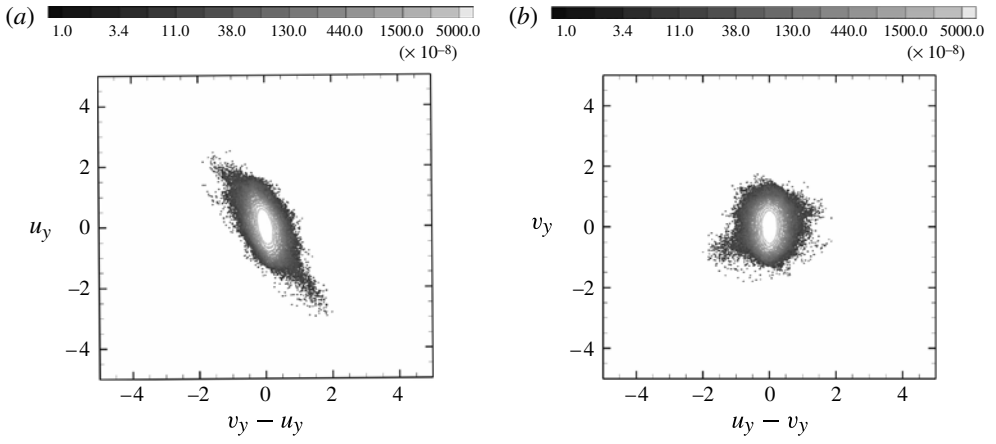

FIGURE 13. Scatter plot of wall-normal velocity components: (*a*) fluid velocity versus slip velocity; (*b*) particle velocity versus slip velocity.

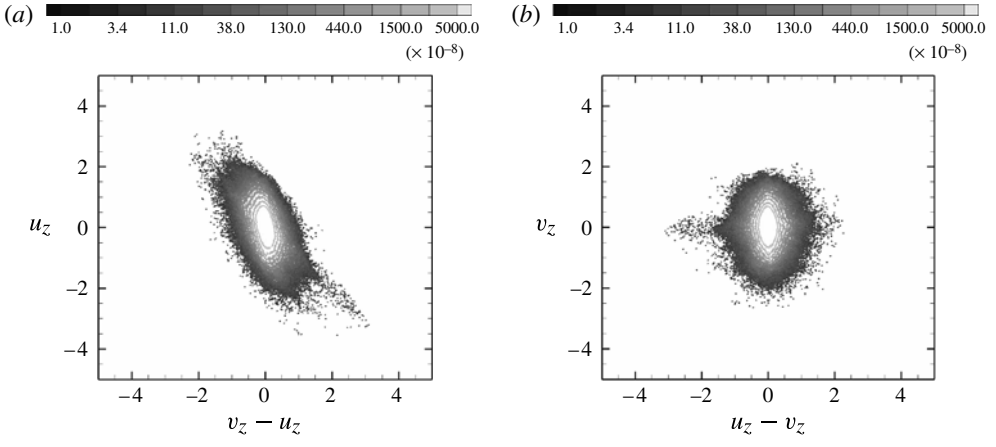

FIGURE 14. Scatter plot of spanwise velocity components: (*a*) fluid velocity versus slip velocity; (*b*) particle velocity versus slip velocity.

power $\overline{\dot{W}_x^P}$ which stems from work done by the fluid on the particles is therefore negative in the buffer layer and viscous sublayer in keeping with figure 9(*b*).

Scatter plots corresponding to those in figure 12 are shown in figures 13 and 14 in terms of the wall-normal and spanwise velocity components, respectively. The covariances between the fluid velocity u_y and the slip velocity $v_y - u_y$ in figure 13(*a*) and between u_z and $v_z - u_z$ in figure 14(*a*) both exhibit distinct asymmetries with dominance from events in the second and fourth quadrants. These asymmetries make $\overline{\dot{W}_y^f}$ and $\overline{\dot{W}_z^f}$ negative, as already shown by the conditionally averaged results in figure 9(*e*,*f*). However, the loss of fluid kinetic energy due to the particle–fluid interactions is not transferred to the particles. The vanishingly small levels of $\overline{\dot{W}_y^P}$ and $\overline{\dot{W}_z^P}$ in figure 9 are fully consistent with the associated scatter plots in figures 13(*b*) and 14(*b*), respectively. The former plot exhibits symmetries about both the v_y-axis

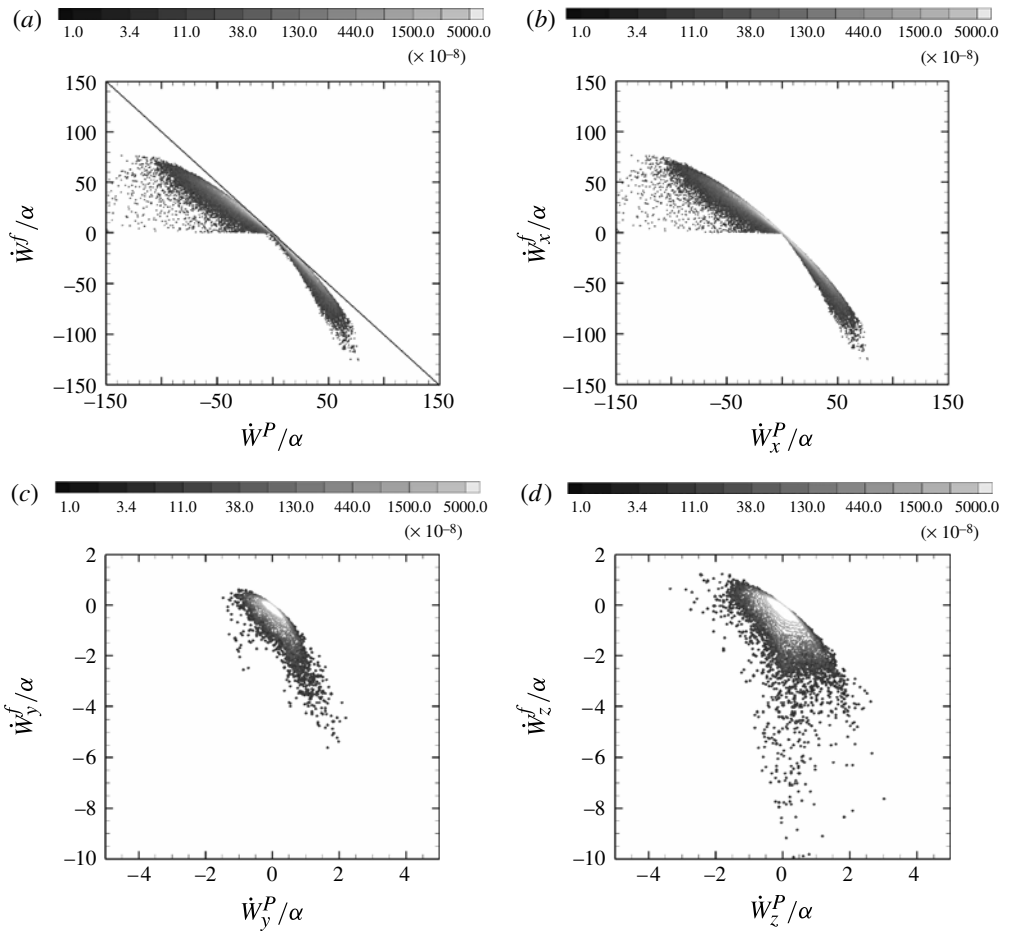

FIGURE 15. Scatter plots of power resulting from work by a particle on the fluid $\dot{W}^f$ versus power due to work by the fluid on the particle $\dot{W}^P$. (*a*) Total power. Events on the straight line $\dot{W}^f = -\dot{W}^P$ correspond to $\varepsilon_P = 0$. (*b*) Power exchange due to streamwise motions; (*c*) power exchange due to wall-normal motions; (*d*) power exchange due to spanwise motions. Notice the different scaling in (*c,d*).

and the $(u_y - v_y)$-axis and the covariance between v_y and $v_y - u_y$ becomes negligibly small. The same arguments apply to the scatter plot in figure 14(*b*). The power transferred from the fluid to the particles by means of cross-sectional motions is therefore negligible, and the loss of fluid kinetic energy is due to particle dissipation rather than interphasial transfer.

Let us finally consider the covariance between the power $\dot{W}^f$ resulting from work by a particle on the fluid versus the power $\dot{W}^P$ resulting from work by the fluid on the particle in figure 15. The straight line $\dot{W}^f = -\dot{W}^P$ in figure 15(*a*) corresponds to $\varepsilon^p = 0$ according to (3.6). By definition, all events are below this line and therefore give rise to particle dissipation. The distance from the line to a point in the scatter plot is a measure of the contribution of that event to the particle dissipation and thereby to the drainage of mechanical energy from the fluid–particle system. The particle dissipation is the result of an imbalance in the power exchange between the particle and the fluid,

i.e. when $\dot{W}^f \neq -\dot{W}^P$. For a modest power exchange, i.e. events close to the origin in figure 15(*a*), the imbalance is also fairly small and so is the particle dissipation. The largest imbalance and thus the greatest particle dissipation rate are associated with events with a substantial power exchange.

The scatter plot of $\dot{W}_x^f$ versus $\dot{W}_x^P$ in figure 15(*b*) is indistinguishable from the plot in figure 15(*a*). We can therefore conclude that the streamwise motions are responsible for almost all of the energy exchange between the particles and the fluid. This is indeed confirmed by the scatter plots of the power exchanges caused by cross-sectional motions in figure 15(*c,d*) when the different scaling on the axes is recognized. The vast majority of events in these two scatter plots are below $\dot{W}_y^f = 0$ and $\dot{W}_z^f = 0$, and the conditionally averaged power transferred from the particles to the fluid becomes distinctly negative, as seen in figure 9(*e,f*). However, as already noticed, the energy exchange associated with the cross-sectional motions is only a small fraction of the energy exchange caused by the streamwise velocity; see e.g. figure 15(*b*).

7. Discussion and concluding remarks

Two-way coupled direct numerical simulations of turbulent channel flow laden with spherical particles have been performed with an Eulerian–Lagrangian point particle approach. Five different cases were designed with a view to studying the influence of the particle response time and the particle loading on the modulations of the turbulent flow field in a fully developed turbulent channel flow. Statistical results showed an attenuation of the Reynolds shear stress and the turbulent velocity fluctuations in the wall-normal and spanwise directions, whereas an augmentation of the velocity fluctuations in the streamwise direction was observed. Such modulations were observed only for relatively high particle loadings, and the deviations from the statistics of the unladen channel flow increased with increasing particle response time. From an engineering viewpoint, it is particularly noteworthy that these modulations of the turbulence field were accompanied by an increasing bulk flow. Since the driving pressure gradient was the same in all simulations, the enhanced flow rate in the particle-laden channel is equivalent to drag reduction.

We intentionally simplified the modelling approach by neglecting forces other than Stokes drag in order to focus on the particle–fluid interactions in two-way coupled simulations. Neglecting gravity makes it difficult to compare the results of the present study with experimental measurements in particle-laden channel flows where gravity comes into play; see e.g. Kaftori, Hetsroni & Banerjee (1995*a*,*b*), Righetti & Romano (2004) and Van Hout (2011). Although gravity may be of importance in channel flows at fairly low Reynolds numbers, as in the present DNS study, one may nevertheless conjecture that the present findings are of practical relevance at higher Reynolds numbers when the role of the particle weight becomes negligible.

Solid particles play two important and independent roles in wall-bounded shear flows. One is as a vehicle to transport turbulent kinetic energy from the core region and into the near-wall layers, and the other is to cause extra energy dissipation. Only the latter has been scrutinized in the present study. The modulations of the turbulence field by the presence of the spherical point particles were analysed in terms of the work performed by the Stokes drag force on the particles and by the corresponding reaction force from the particles on the fluid. A slip velocity between a particle and the local fluid arises due to particle inertia. This slip velocity creates an imbalance between the work performed by the particles on the fluid and the work exerted by the fluid on the particles. The local fluid exerts work on the particles in the core region of

the channel whereas the particles perform work on the fluid in the buffer region and the viscous sublayer. As an outcome of this imbalance, kinetic energy is drained from the fluid–particle suspension by means of so-called particle dissipation.

By decomposing the turbulent velocity field into mean and fluctuating parts, we found that the enhancement of streamwise turbulence was caused by the work done by particles on the local fluid. The extra energy dissipation, which is due to the particle–fluid interactions, was not sufficient to prevent the streamwise intensity from increasing. The velocity fluctuations in the two other directions, however, were substantially damped. The physical mechanisms responsible for the turbulence modulations caused by the presence of tiny point particles have been elucidated by means of conventional and conditionally averaged statistical data and instantaneous scatter plots of the fluctuating fluid or particle velocity versus the fluctuating slip velocity.

The presence of inertial particles provides an extra drain of energy from the suspension, in addition to the viscous energy dissipation caused by small-scale turbulent motions. Irrespective of whether the particles receive or lose energy from the fluid, the particle dissipation will always give rise to a loss of mechanical energy from the fluid–particle system as long as a slip velocity exists. This energy loss may even cause significant drag reduction.

Acknowledgements

This work has been supported by A/S Norske Shell through a research fellowship (contract 4610020178/C08156) and by The Research Council of Norway (Programme for Supercomputing) through a grant of computing time. The research work reported in this paper also benefited from scientific interactions facilitated by COST Action FP1005 funded by the European Science Foundation.

REFERENCES

BALACHANDAR, S. & EATON, J. K. 2010 Turbulent dispersed multiphase flow. *Annu. Rev. Fluid Mech.* **42**, 111–133.

BIJLARD, M. J., OLIEMANS, R. V. A., PORTELA, L. M. & OOMS, G. 2010 Direct numerical simulation analysis of local flow topology in a particle-laden turbulent channel flow. *J. Fluid Mech.* **653**, 35–56.

DRITSELIS, C. D. & VLACHOS, N. S. 2008 Numerical study of educed coherent structures in the near-wall region of a particle-laden channel flow. *Phys. Fluids* **20**, 055103.

DRITSELIS, C. D. & VLACHOS, N. S. 2011 Numerical investigation of momentum exchange between particles and coherent structures in low Re turbulent channel flow. *Phys. Fluids* **23**, 025103.

EATON, J. K. & FESSLER, J. R. 1994 Preferential concentration of particles by turbulence. *Intl J. Multiphase Flow* **20**, 169–209.

ELGHOBASHI, S. & TRUESDELL, G. C. 1993 On the two-way interaction between homogeneous turbulence and dispersed solid particles. Part 1. Turbulence modification. *Phys. Fluids* A **5**, 1790–1801.

GILLISSEN, J. J. J., BOERSMA, B. J., MORTENSEN, P. H. & ANDERSSON, H. I. 2008 Fibre-induced drag reduction. *J. Fluid Mech.* **602**, 209–218.

GORE, R. A. & CROWE, C. T. 1989 The effect of particle size on modulating turbulent intensity. *Intl J. Multiphase Flow* **15**, 279–285.

HANJALIC, K. & LAUNDER, B. 2011 *Modelling Turbulence in Engineering and the Environment*. Cambridge University Press.

HUSSAINOV, M., KARTUSHINSKY, A., RUDI, Ü., SHCHEGLOV, I., KOHNEN, G. & SOMMERFELD, M. 2000 Experimental investigation of turbulence modulation by solid particles in a grid-generated vertical flow. *Intl J. Heat Fluid Flow* **21**, 365–373.

KAFTORI, D., HETSRONI, G. & BANERJEE, S. 1995*a* Particle behaviour in the turbulent boundary layer. Part 1. Motion, deposition and entrainment. *Phys. Fluids* **7**, 1095–1106.

KAFTORI, D., HETSRONI, G. & BANERJEE, S. 1995*b* Particle behaviour in the turbulent boundary layer. Part 2. Velocity and distribution profiles. *Phys. Fluids* **7**, 1107–11221.

KULICK, J. D., FESSLER, J. R. & EATON, J. K. 1994 Particle response and turbulence modification in fully developed channel flow. *J. Fluid Mech.* **277**, 109–134.

LI, Y., MCLAUGHLIN, J. B., KONTOMARIS, K. & PORTELA, L. 2001 Numerical simulation of particle-laden turbulent channel flow. *Phys. Fluids* **13**, 2957–2976.

MORTENSEN, P. H., ANDERSSON, H. I., GILLISSEN, J. J. J. & BOERSMA, B. J. 2007 Particle spin in a turbulent shear flow. *Phys. Fluids* **19**, 078109.

MORTENSEN, P. H., ANDERSSON, H. I., GILLISSEN, J. J. J. & BOERSMA, B. J. 2008 Dynamics of prolate ellipsoidal particles in a turbulent channel flow. *Phys. Fluids* **20**, 093302.

PAN, Y. & BANERJEE, S. 1996 Numerical simulation of particle interactions with wall turbulence. *Phys. Fluids* **8**, 2733–2755.

PICCIOTTO, M., GIUSTI, A., MARCHIOLI, C. & SOLDATI, A. 2006 Turbulence modulation by micro-particles in boundary layers. In *IUTAM Symposium on Computational Approaches to Multiphase Flow* (ed. S. Balachandar & A. Prosperetti), pp. 53–62. Springer.

RANI, S. L., WINKLER, C. M. & VANKA, S. P. 2004 Numerical simulations of turbulence modulation by dense particles in a fully developed pipe flow. *Powder Technol.* **141**, 80–99.

RASHIDI, M., HETSRONI, G. & BANERJEE, S. 1990 Particle–turbulence interaction in a boundary layer. *Intl J. Multiphase Flow* **16**, 935–949.

RIGHETTI, M. & ROMANO, G. P. 2004 Particle–fluid interactions in a plane near-wall turbulent flow. *J. Fluid Mech.* **505**, 93–121.

ROSSETTI, S. J. & PFEFFER, R 1972 Drag reduction in dilute flowing gas–solid suspensions. *AIChE J.* **18**, 31–39.

SQUIRES, K. D. & EATON, J. K. 1990 Particle response and turbulence modification in isotropic turbulence. *Phys. Fluids* A **2**, 1191–1203.

TANAKA, T. & EATON, J. K. 2008 Classification of turbulence modification by dispersed spheres using a novel dimensionless number. *Phys. Rev. Lett.* **101**, 114502.

TRUESDELL, G. C. & ELGHOBASHI, S. 1994 On the two-way interaction between homogeneous turbulence and dispersed solid particles. Part 2. Particle dispersion. *Phys. Fluids* **6**, 1405–1407.

VAN HOUT, R. 2011 Time-resolved PIV measurements of the interaction of polystyrene beads with near-wall-coherent structures in a turbulent channel flow. *Intl J. Multiphase Flow* **37**, 346–357.

VREMAN, A. W. 2007 Turbulence characteristics of particle-laden pipe flow. *J. Fluid Mech.* **584**, 235–279.

YAMAMOTO, Y., POTTHOFF, M., TANAKA, T., KAJISHIMA, T. & TSUJI, Y. 2001 Large-eddy simulation of turbulence gas-particle flow in a vertical channel: effect of considering inter-particle collisions. *J. Fluid Mech.* **442**, 303–334.

ZHAO, L. H. & ANDERSSON, H. I. 2011 On particle spin in two-way coupled turbulent channel flow simulations. *Phys. Fluids* **23**, 093302.

ZHAO, L. H. & ANDERSSON, H. I. 2012 Statistics of particle suspensions in turbulent channel flow. *Commun. Comput. Phys.* **11**, 1311–1322.

ZHAO, L. H., ANDERSSON, H. I. & GILLISSEN, J. J. J. 2010 Turbulence modulation and drag reduction by spherical particles. *Phys. Fluids* **22**, 081702.

ZHAO, L. H., MARCHIOLI, C. & ANDERSSON, H. I. 2012 Stokes number effects on particle slip velocity in wall-bounded turbulence and implications for dispersion models. *Phys. Fluids* **24**, 021705.